Tutorial

Sander Konijnenberg*

An introduction to the theory of ptychographic phase retrieval methods

https://doi.org/10.1515/aot-2017-0049
Received July 28, 2017; accepted October 9, 2017; previously published online November 9, 2017

Abstract: An overview of several ptychographic phase retrieval methods and the theory behind them is presented. By looking into the theory behind more basic single-intensity pattern phase retrieval methods, a theoretical framework is provided for analyzing ptychographic algorithms. Extensions of ptychographic algorithms that deal with issues such as partial coherence, thick samples, or uncertainties of the probe or probe positions are also discussed. This introduction is intended for scientists and students without prior experience in the field of phase retrieval or ptychography to quickly get introduced to the theory, so that they can put the more specialized literature in context more easily.

Keywords: coherent diffractive imaging; lensless imaging; phase retrieval; ptychography.

1 Introduction

Electromagnetic radiation has long been an invaluable tool to observe many different objects and phenomena. For example, we navigate the world every day using our eyes to detect light, but a much broader range of the electromagnetic spectrum can be used to study many more phenomena: X-rays can be used to study the molecular structure of crystals, while infrared radiation is observed to reveal the history of the universe. It is, therefore, important to notice that with all our current detectors, we can detect only part of the information that is encoded in electromagnetic fields: we can measure how strong the field is, but we cannot directly measure each point in that field oscillates with respect to each other if the field oscillates at optical frequencies or higher. Put mathematically, if we have a monochromatic coherent field, we can describe it with a complex-valued function $U=|U|e^{i\phi}$, but we can only measure directly its intensity $|U|^2$, and not its phase ϕ.

One can use tricks to make intensity patterns reveal information about the phase, for example, using interferometry. In this case, one has two fields $U_1=|U_1|e^{i\phi_1}$ and $U_2=|U_2|e^{i\phi_2}$, which are made to interfere. The observed intensity can be written as

$$|U_1+U_2|^2=|U_1|^2+|U_2|^2+2|U_1||U_2|\cos(\phi_1-\phi_2), \quad (1)$$

where we now can see that the phases ϕ_1 and ϕ_2 affect the observed intensity. Interferometric techniques have proven to be extremely useful in, for example, surface height measurements (where white light interferometry is used) and three-dimensional (3D) imaging (where optical coherence tomography is used). However, a drawback of interferometric setups is that they can be bulky and may be rather sensitive to perturbations. In fact, this sensitivity has been exploited to detect the extremely weak perturbations caused by gravitational waves. For other applications such as phase imaging, it is more convenient to use less sophisticated and sensitive setups, so other methods such as Zernike phase-contrast microscopy have been developed.

When tremendous computational power became available with the advent of computers, another field of phase retrieval emerged, namely, computational phase retrieval. The overall trend in this development is that the difficulties are moved from the experiment to the computational domain: the experimental setup gets simpler, while the phase retrieval algorithms become more sophisticated. For example, with coherent diffractive imaging (CDI), it is possible to create an image of an object without having to use any high-quality lenses. By simply measuring the intensity pattern of the scattered far field, the complex-valued transmission function of the object can be computed using iterative phase retrieval algorithms. This is, for example, useful for imaging using wavelengths in the soft X-ray regime, for which the quality of the focusing optics is limited.

***Corresponding author: Sander Konijnenberg,** Optics Research Group, Delft University of Technology, Delft 2628 CH, The Netherlands, e-mail: a.p.konijnenberg@tudelft.nl

One particular method of phase retrieval that has recently gained notable popularity and success is ptychography. In this method, an object is illuminated by a spot (referred to as 'the probe') that is shifted to different positions that are chosen such that the probe at adjacent positions overlap. For each position, the far-field intensity pattern is recorded, and the object's complex-valued transmission function is computed iteratively using these patterns. Because the probes overlap, there is a degree of redundancy in the measured diffraction patterns, which makes the reconstruction scheme very robust. In fact, it has been proven to be so robust that much more than just the object can be reconstructed. To name a few: uncertainties in the probe and probe positions can be corrected; 3D information of the object can be reconstructed; coherence properties of the illuminating probe can be obtained. In the following, we will have a closer look at how the ptychographic algorithm works and in what ways it has been extended. Though we try to give a good overview of the field, it will be far from exhaustive, given the large numbers of variations that have been invented and are still being invented at a considerable rate.

First, we discuss the single-intensity phase retrieval problem. We will see that there are two ways to approach this problem: as a cost-minimization problem or as a feasibility problem. These two approaches will then be used to study ptychographic phase retrieval algorithms. Next, we discuss several variations of the ptychographical algorithm that deal with issues such as probe retrieval, position correction, partial coherence, and thick samples.

2 Single-intensity phase retrieval algorithms

Although the focus of this review lies on ptychographical algorithms, one ought to first familiarize oneself with simpler phase retrieval algorithms that use a single-intensity pattern before studying ptychography. The problem we consider is the following: we have a object with a complex-valued transmission function $\psi(\mathbf{x})$, where $\mathbf{x}$ is a 2D position vector. We denote its Fourier transform as $\Psi(\mathbf{x}')$, so we can write the intensity pattern that is measured in the far field as $|\Psi(\mathbf{x}')|^2$. In addition, we suppose that the object has a finite support S, which we know:

$$\psi(\mathbf{x}) = 0 \quad \text{if} \quad \mathbf{x} \notin S. \tag{2}$$

Thus, we have two known constraints in the two domains:
1. a *support constraint* S in the object domain;
2. an *amplitude constraint* $|\Psi(\mathbf{x}')|$ in the Fourier domain.

The situation is illustrated in Figure 1. A straightforward and intuitive algorithm to find $\psi(\mathbf{x})$ would be to alternately apply these two constraints, which gives the *error reduction* (ER) algorithm [1]
1. For the k^{th} estimate $f_k(\mathbf{x})$, calculate its Fourier transform $F_k(\mathbf{x}')$.
2. Set the amplitude of the estimated Fourier transform equal to the measured amplitude $|\Psi(\mathbf{x}')|$ while keeping the phase of the estimate.

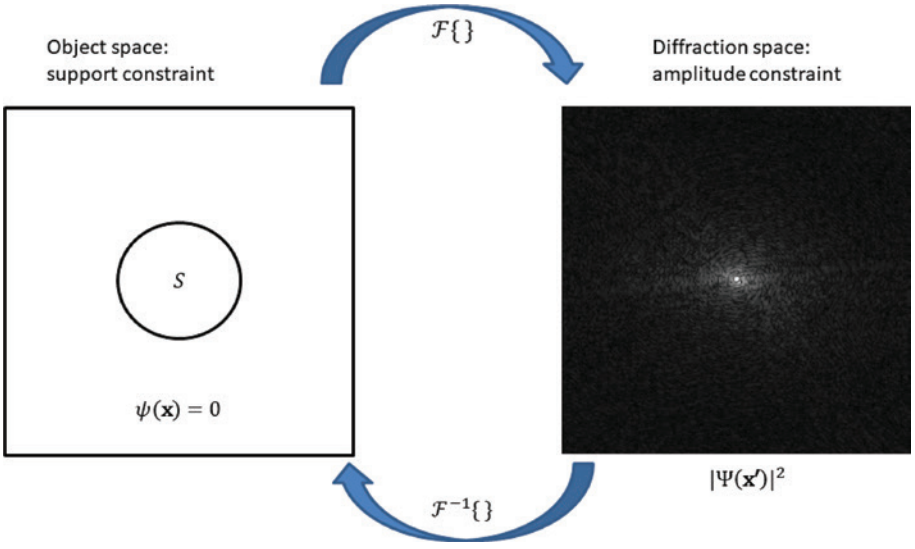

Figure 1: The single-intensity phase retrieval problem uses two constraints in different spaces: a support constraint in object space and a modulus constraint in diffraction space. The two spaces are related to each other by a Fourier transform.

$$F_k^{\text{upd}}(\mathbf{x}') = \frac{F_k(\mathbf{x}')}{|F_k(\mathbf{x}')|}|\Psi(\mathbf{x}')|. \tag{3}$$

3. Inverse Fourier transform the updated field $F_k^{\text{upd}}(\mathbf{x}')$ to obtain

$$f_k^{\text{upd}}(\mathbf{x}) = \mathcal{F}^{-1}\{F_k^{\text{upd}}(\mathbf{x}')\}(\mathbf{x}). \tag{4}$$

4. Apply the support constraint to $f_k^{\text{upd}}(\mathbf{x})$ to obtain the new object estimate $f_{k+1}(\mathbf{x})$:

$$f_{k+1}(\mathbf{x}) = \begin{cases} f_k^{\text{upd}}(\mathbf{x}) & \text{if } \mathbf{x} \in S, \\ 0 & \text{if } \mathbf{x} \notin S. \end{cases} \tag{5}$$

There are two different ways in which we can interpret this intuitive scheme mathematically (illustrated in Figure 2):

As a **feasibility problem**. We define two sets: a set A, which consists of all functions $f(\mathbf{x})$ that satisfy the support constraint

$$A = \{f(\mathbf{x}) : f(\mathbf{x}) = 0 \text{ if } \mathbf{x} \notin S\}, \tag{6}$$

and a set B, which consists of all $f(\mathbf{x})$ whose Fourier transforms $F(\mathbf{x}')$ satisfy the modulus constraint

$$B = \{f(\mathbf{x}) : |F(\mathbf{x}')| = |\Psi(\mathbf{x}')|\}. \tag{7}$$

To solve the phase retrieval problem, we try to find an $f(\mathbf{x})$ that satisfies both constraints

$$f(\mathbf{x}) \in A \cap B. \tag{8}$$

We can find this intersection using the *alternating projection* method. We can define P_A and P_B to be the operators that project a function $f(\mathbf{x})$ onto A and B, respectively. More explicitly,

$$\begin{aligned} P_A f(\mathbf{x}) &= f(\mathbf{x})\mathbf{1}_{\mathbf{x}\in S}, \\ P_B f(\mathbf{x}) &= \mathcal{F}^{-1}\left\{\frac{F(\mathbf{x}')}{|F(\mathbf{x}')|}|\Psi(\mathbf{x}')|\right\}, \end{aligned} \tag{9}$$

where $\mathcal{F}^{-1}\{\cdot\}$ denotes the inverse Fourier transform, and

$$\mathbf{1}_{\mathbf{x}\in S} = \begin{cases} 1 & \text{if } \mathbf{x} \in S, \\ 0 & \text{if } \mathbf{x} \notin S. \end{cases} \tag{10}$$

We can write an ER iteration as

$$f_{k+1}(\mathbf{x}) = P_A P_B f_k(\mathbf{x}). \tag{11}$$

This method tends to be successful when A and B are convex sets, but in our problem, B is unfortunately not a convex set. To see this, note that if, for example, $|\Psi(\mathbf{x}')| = a$, then $f_1(\mathbf{x})$ and $f_2(\mathbf{x})$ for which $F_1(\mathbf{x}') = a$ and $F_2(\mathbf{x}') = -a$ both lie in B, but the convex combination $\frac{1}{2}f_1(\mathbf{x}) + \frac{1}{2}f_2(\mathbf{x}) = 0$ does not.

As a **cost-minimization problem** [2]. We can define $f(\mathbf{x})$ to be an object estimate, and we define $F(\mathbf{x}')$ to be the Fourier transform of the portion of $f(\mathbf{x})$ that lies within S:

$$F(\mathbf{x}') = \sum_{\mathbf{x}} f(\mathbf{x}) e^{-2\pi i \mathbf{x}'\cdot\mathbf{x}} \mathbf{1}_{\mathbf{x}\in S}\Delta, \tag{12}$$

where Δ represents the pixel spacing. To reconstruct $\psi(\mathbf{x})$ from the measured intensity, we want to minimize the difference between the measured amplitude $|\Psi(\mathbf{x}')|$ and the reconstructed amplitude $|F(\mathbf{x}')|$. Thus, we can introduce the cost function

$$L[f(\mathbf{x})] = \sum_{\mathbf{x}'} (|F(\mathbf{x}')| - |\Psi(\mathbf{x}')|)^2, \tag{13}$$

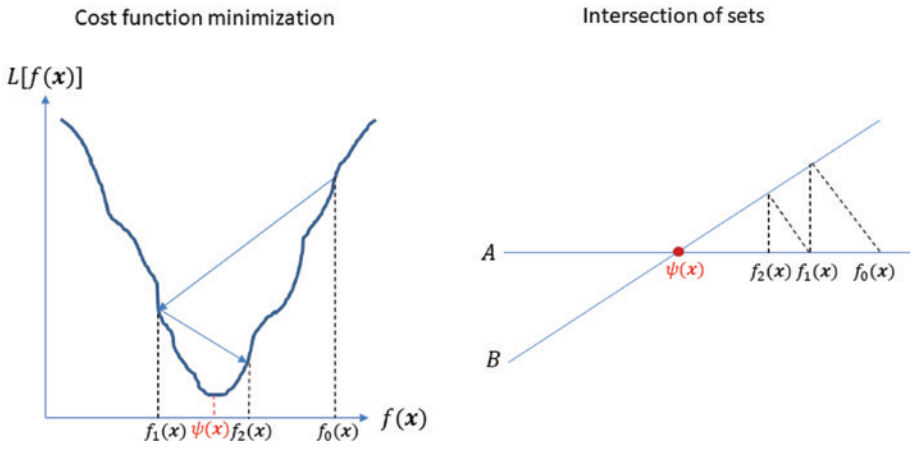

Figure 2: The phase retrieval problem can be formulated as a cost function minimization problem or as a feasibility problem.

which we want to minimize. To do this, we can use the *gradient descent scheme* where we update the object estimate according to

$$f_{k+1}(\mathbf{x}) = f_k(\mathbf{x}) - \mu \frac{\partial L}{\partial f(\mathbf{x})^*}. \tag{14}$$

Here, μ is a step that can be chosen freely, and $\frac{\partial L}{\partial f(\mathbf{x})^*}$ is a Wirtinger derivative. It can be shown that the steepest ascent of L points to the direction of $\frac{\partial L}{\partial f(\mathbf{x})^*}$ [3]. Noting that

$$\frac{\partial |F(\mathbf{x}')|}{\partial F(\mathbf{x}')^*} = \frac{\partial \sqrt{F(\mathbf{x}')F(\mathbf{x}')^*}}{\partial F(\mathbf{x}')^*} = \frac{F(\mathbf{x}')}{2|F(\mathbf{x}')|}$$

and

$$\frac{\partial F(\mathbf{x}')^*}{\partial f(\mathbf{x})^*} = e^{2\pi i \mathbf{x}'\cdot\mathbf{x}} \mathbf{1}_{\mathbf{x}\in S} \Delta \tag{15}$$

we find that

$$\begin{aligned} \frac{\partial L}{\partial f(\mathbf{x})^*} &= \sum_{\mathbf{x}'} \left(F(\mathbf{x}') - \frac{F(\mathbf{x}')}{|F(\mathbf{x}')|} |\Psi(\mathbf{x}')| \right) e^{2\pi i \mathbf{x}'\cdot\mathbf{x}} \mathbf{1}_{\mathbf{x}\in S} \Delta \\ &= (f_k(\mathbf{x}) - f_k^{\mathrm{upd}}(\mathbf{x})) \mathbf{1}_{\mathbf{x}\in S}, \end{aligned} \tag{16}$$

where $f_k^{\mathrm{upd}}(\mathbf{x})$ is defined as in Eq. (4). If we choose $\mu = 1$ in Eq. (14), we get

$$f_{k+1}(\mathbf{x}) = f_k^{\mathrm{upd}}(\mathbf{x}) \mathbf{1}_{\mathbf{x}\in S}, \tag{17}$$

which is the same as Eqs. (5) and (11).

So we see that the ER algorithm can be interpreted as solving a feasibility problem using the method of alternate projections or as solving a cost minimization problem using the steepest descent method with a step size of $\mu = 1$. Note that for general μ, we can write the steepest descent update function as

$$\begin{aligned} f_{k+1}(\mathbf{x}) &= f_k(\mathbf{x}) - \mu(f_k(\mathbf{x}) - f_k^{\mathrm{upd}}(\mathbf{x})) \mathbf{1}_{\mathbf{x}\in S} \\ &= (1-\mu) f_k(\mathbf{x}) + \mu f_k^{\mathrm{upd}}(\mathbf{x}) \mathbf{1}_{\mathbf{x}\in S} \\ &= (1-\mu) f_k(\mathbf{x}) + \mu P_A P_B f_k(\mathbf{x}). \end{aligned} \tag{18}$$

Thus, we see that also with the method of alternate projections, we can introduce an equivalent of a step size. To visualize what this means, observe that we can write

$$f_{k+1}(\mathbf{x}) = P_A((1-\mu)I + \mu P_B) f_k(\mathbf{x}), \tag{19}$$

where I denotes the identity operator. Thus, compared to the case where $\mu = 1$, we have substituted P_B with $(1-\mu)I + \mu P_B$. While P_B sets the amplitude of the estimated diffracted field $F(\mathbf{x}')$ equal to the measured amplitude $|\Psi(\mathbf{x}')|$ by moving $F(\mathbf{x}')$ to $\frac{F(\mathbf{x}')}{|F(\mathbf{x}')|}|\Psi(\mathbf{x}')|$, the operator $(1-\mu)I + \mu P_B$ moves $F(\mathbf{x}')$ in the direction of $\frac{F(\mathbf{x}')}{|F(\mathbf{x}')|}|\Psi(\mathbf{x}')|$ with a step size that depends on μ. This interpretation is illustrated in Figure 3. Similar projection operators have been derived in Ref. [4] from a maximum likelihood principle with the aim to improve noise robustness.

It is important to be aware of these two different interpretations because even though they end up giving the same algorithm, they give us different hints as to how the algorithm can be improved and extended (which is very much necessary because while the ER algorithm is simple and intuitive, it also suffers from major stagnation issues). For example, when interpreting the phase retrieval problem as a feasibility problem, one can draw inspiration from other methods for convex optimization, which led to many improved algorithms [5], such as the difference map (DM) [6] and relaxed averaged alternating reflection (RAAR) algorithms [7]. A very popular phase retrieval algorithm, the hybrid input-output (HIO) algorithm [1], was originally not invented through such reasoning, but it was later demonstrated to be an instance of the Douglas-Rachford algorithm [8]. When interpreting the phase retrieval problem as a cost-minimization problem, one could experiment with choosing different cost functions [9, 10], choosing a different step size [11], or using update schemes other than the steepest descent method (such as the conjugate gradient method or Newton's method) [12]. For example, it has been demonstrated that reducing the step size of the update function significantly improves the noise robustness [11] of the algorithm.

2.1 Resolution: detector size, dynamic range, and background noise

When imaging a sample, it is always important to know with what resolution it can be imaged. In standard

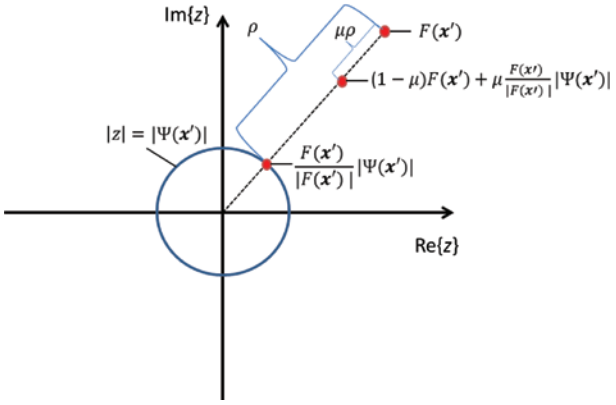

Figure 3: Illustration of the meaning of the step size μ in the context of the method of alternate projections.

microscopes, the resolution is determined by the numerical aperture (NA) of the focusing optics, but in diffractive imaging, we do not use lenses to form the image. Instead, we use the diffraction patterns, which correspond to the spatial Fourier transform of the object. The resolution with which we can reconstruct the sample, thus, depends on the highest spatial frequency we can capture with the detector. There are, roughly speaking, two factors that limit the spatial frequencies we can detect:

1. The finite size of the detector. The part of the diffraction pattern that fall outside of the detector cannot be used in the reconstruction. Thus, while in a standard microscope the resolution is determined by the NA of the focusing optics, in diffractive imaging, the resolution is determined by the NA of the detector (although for ptychography, it has been demonstrated that extrapolation of the diffraction pattern beyond the detector NA is possible [13]).
2. The noise level of the detector and the dynamic range of the diffraction pattern. If the object is rather smooth, the diffraction pattern tends to have a very sharp central peak, while the higher spatial frequencies have a much lower amplitude. If the amplitude is so low that they fall below the noise level of the detector, we are basically cutting off these higher spatial frequencies.

In order to reduce the negative effects of a high dynamic range, several methods are being implemented. One could block the central peak with a beam stop so that one can increase the exposure time to capture the higher spatial frequencies without causing saturation by the central peak [14], as is illustrated in Figure 4. Alternatively, one could use a diffuser or curved illumination to decrease the dynamic range of the diffraction pattern [15–17]. Another common issue in CDI that affects the reconstruction quality is background noise, and several methods have been proposed for background noise removal [18, 19].

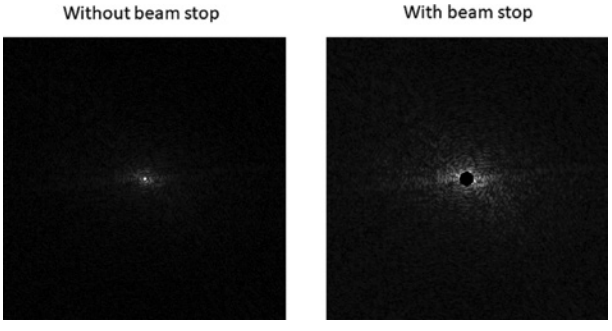

Figure 4: Using a beam stop to block the zero-order diffraction peak is one way to reduce the dynamic range of the measurement, thereby, allowing more information of higher spatial frequencies to be captured.

3 Ptychographical phase retrieval algorithms

3.1 Regular ptychography

We have discussed a phase retrieval algorithm that reconstructs an exit wave $\psi(\mathbf{x})$ with a known support S and Fourier amplitude $|\Psi(\mathbf{x}')|$. In ptychography, we have multiple exit waves that are obtained by illuminating an unknown object $O(\mathbf{x})$ with a known probe $P(\mathbf{x})$ that is shifted to different positions $\mathbf{X}_j$

$$\psi_j(\mathbf{x}) = O(\mathbf{x})P(\mathbf{x}-\mathbf{X}_j). \tag{20}$$

For each $\psi_j(\mathbf{x})$, we measure the Fourier intensity $|\Psi_j(\mathbf{x}')|^2$, as is shown in Figure 5. So whereas for the single-intensity phase retrieval algorithm we have a support constraint, for ptychography, we have the constraint that the exit waves $\psi_j(\mathbf{x})$ can factorize into a single object function $O(\mathbf{x})$ and a shifting probe $P(\mathbf{x}-\mathbf{X}_j)$. As a special case, we could create a probe by illuminating an aperture with a plane wave, in which case each $\psi_j(\mathbf{x})$ has a support constraint as $P(\mathbf{x}-\mathbf{X}_j)$ is a step function. Thus, we can intuitively come up with a basic ptychographic reconstruction

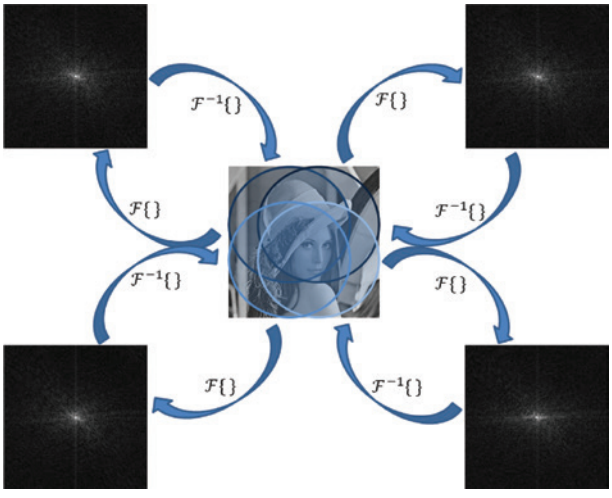

Figure 5: In the ptychographic phase retrieval problem, an illuminating probe is shifted to different overlapping positions across the object. For each position, a diffraction pattern is recorded, and using these diffraction patterns together with the prior knowledge of the probe and probe positions, the object can be reconstructed.

algorithm that draws inspiration from the ER algorithm that we discussed previously

1. Given a k^{th} object estimate $O_k(\mathbf{x})$, calculate the estimated exit wave for a certain j
$$f_{k,j}(\mathbf{x}) = O_k(\mathbf{x})P(\mathbf{x}-\mathbf{X}_j). \tag{21}$$
2. Calculate the update of the estimated exit wave $f_{k,j}^{\text{upd}}(\mathbf{x})$ according to Eq. (4).
3. Update the object estimate by dividing out the probe from the updated exit wave. However, because $\frac{f_{k,j}^{\text{upd}}(\mathbf{x})}{P(\mathbf{x}-\mathbf{X}_j)}$ can diverge, instead, update the object as
$$O_k(\mathbf{x}) := \frac{P^*(\mathbf{x}-\mathbf{X}_j)f_{k,j}^{\text{upd}}(\mathbf{x})}{|P(\mathbf{x}-\mathbf{X}_j)|^2+\alpha}. \tag{22}$$
Here, α is a small parameter to avoid division by 0.
4. Do this procedure for all j to complete one iteration, after which, k is increased to $k+1$.

In case $P(\mathbf{x})$ is a step function, we are basically applying ER iterations for all probe positions sequentially. If the probe positions are chosen such that the probes at adjacent probe positions overlap sufficiently (approximately 60% to 85% overlap [20]), each ER update at one position helps the reconstruction at adjacent positions. Because of these interconnections, the ptychographic reconstruction is quite robust, even though the ER algorithm, by itself, suffers severely from stagnation problems.

We have seen previously how the ER algorithm can be derived more systematically and how this helps us to improve it. Let us, therefore, similarly consider ptychography more systematically.

As a **feasibility problem**. Let us denote the collection of exit waves $f_j(\mathbf{x})$ as $\mathbf{f}$. We define two sets: a set A, which consists of all $\mathbf{f}$ that satisfy the factorization constraint
$$\begin{aligned} A = \{\mathbf{f} &: \text{there exists an } O(x) \text{ such that } f_j(\mathbf{x}) \\ &= O(\mathbf{x})P(\mathbf{x}-\mathbf{X}_j) \text{ for all } j\}, \end{aligned} \tag{23}$$
and a set B, which consists of all $\mathbf{f}$ that satisfy the modulus constraints
$$B = \{\mathbf{f} : |F_j(\mathbf{x}')| = |\Psi_j(\mathbf{x}')| \text{ for all } j\}. \tag{24}$$

We define P_A and P_B to be the projection operators that project an $\mathbf{f}$ onto A and B, respectively [21]:
$$\begin{aligned} &(P_A\mathbf{f})_j = O_{\mathbf{f}}(\mathbf{x})P(\mathbf{x}-\mathbf{X}_j) \quad \text{where} \quad O_{\mathbf{f}}(\mathbf{x}) = \frac{\sum_{j'} f_{j'}(\mathbf{x})P(\mathbf{x}-\mathbf{X}_{j'})^*}{\alpha+\sum_{j'}|P(\mathbf{x}-\mathbf{X}_{j'})|^2}, \\ &(P_B\mathbf{f})_j = \mathcal{F}^{-1}\left\{\frac{F_j(\mathbf{x}')}{|F_j(\mathbf{x}')|}|\Psi(\mathbf{x}')|\right\}, \end{aligned} \tag{25}$$
where α is a small parameter to prevent division by 0. To solve the ptychographic phase retrieval problem, we try to find an $\mathbf{f}$ that satisfies both constraints
$$\mathbf{f} \in A \cap B, \tag{26}$$
and from this $\mathbf{f}$, we can use the expression for $O_{\mathbf{f}}(\mathbf{x})$ in Eq. (25) to calculate $O(\mathbf{x})$. To find such an $\mathbf{f}$, one can apply an alternate projection scheme
$$\mathbf{f}_{k+1} = P_A P_B \mathbf{f}_k, \tag{27}$$
or any other projection-based scheme such as HIO, RAAR, or DM.

As a **cost-minimization problem** [22, 23]. Given an estimated object $O_k(\mathbf{x})$, we can calculate the estimated Fourier amplitudes $|F_j(\mathbf{x}')|$, which, for a good reconstruction, need to be the same as the measured Fourier amplitudes $|\Psi_j(\mathbf{x}')|$. Thus, we can introduce a cost function
$$L[O_k(\mathbf{x})] = \sum_j \sum_{\mathbf{x}'} (|F_j(\mathbf{x}')| - |\Psi_j(\mathbf{x}')|)^2, \tag{28}$$
which we want to minimize. Using the steepest descent scheme, we get
$$\begin{aligned} O_{k+1}(\mathbf{x}) &= O_k(\mathbf{x}) - \mu \frac{\partial L}{\partial O_k(\mathbf{x})^*} \\ &= O_k(\mathbf{x}) - \mu \sum_j P(\mathbf{x}-\mathbf{X}_j)^* (f_{k,j}(\mathbf{x}) - f_{k,j}^{\text{upd}}(\mathbf{x})). \end{aligned} \tag{29}$$

It is also possible to use a preconditioner so that the update function changes to, for example [12],
$$O_{k+1}(\mathbf{x}) = O_k(\mathbf{x}) - \mu \frac{\sum_j P(\mathbf{x}-\mathbf{X}_j)^* (f_{k,j}(\mathbf{x}) - f_{k,j}^{\text{upd}}(\mathbf{x}))}{\sum_j |P(\mathbf{x}-\mathbf{X}_j)|^2}. \tag{30}$$

A major difference between the update scheme in Eq. (22) and the update schemes in Eqs. (27) and (29) is that the latter two update the object *globally* (i.e. the updates for all probe positions are used to update the object estimate in its entirety at once), whereas the former updates the object *incrementally* (i.e. the object estimate is updated for each probe position sequentially). Using an incremental approach may be preferred when the number of recorded intensity patterns is very large, which would make a global update iteration very costly [11]. With an incremental update scheme and the right preconditioner and step size, one can obtain the update scheme of Eq. (22) using the steepest descent algorithm. Another regularized update function has been proposed more recently [24]:
$$O_k(\mathbf{x}) := O_k(\mathbf{x}) - \mu \frac{P(\mathbf{x}-\mathbf{X}_j)^* (f_{k,j}(\mathbf{x}) - f_{k,j}^{\text{upd}}(\mathbf{x}))}{(1-\alpha)|P(\mathbf{x}-\mathbf{X}_j)|^2 + \alpha \max|P(\mathbf{x}-\mathbf{X}_j)|^2}, \tag{31}$$

where μ and α are update parameters. Moreover, this algorithm has been extended by adding 'momentum' to the update. Extension of the gradient descent method using momentum, as well as other extensions of the gradient descent algorithm are explained in Ref. [25].

Advanced projection-based methods have been explored using global updates [12, 21], as well as using incremental methods [26].

3.2 Fourier ptychography

In Fourier ptychography [27], the Fourier transform of $O(\mathbf{x})$ takes on the role of the object that we need to reconstruct. Let us denote the Fourier transform of $O(\mathbf{x})$ as $\hat{O}(\mathbf{x}')$. We can create $\hat{O}(\mathbf{x}')$ by illuminating the object with a plane wave and focusing the transmitted field with a lens, after which $\hat{O}(\mathbf{x}')$ forms in the focal plane. By tilting the angle of the incident plane wave, $\hat{O}(\mathbf{x}')$ is shifted to $\hat{O}(\mathbf{x}'+\mathbf{X}_j')$. By putting a fixed aperture in the focal plane, we multiply $\hat{O}(\mathbf{x}'+\mathbf{X}_j')$ by a probe function $\hat{P}(\mathbf{x}')$. The field that is transmitted by the aperture can then be Fourier transformed by a second lens (Figure 6). $\hat{P}(\mathbf{x}')$ can also describe aberrations introduced by this second lens. By measuring the intensity in the focal plane of the second lens, and changing the angle of the plane wave that is incident on the object, we obtain a ptychographic data set with which we can reconstruct $\hat{O}(\mathbf{x}')$. By inverse Fourier transforming the reconstruction, we obtain a reconstruction for $O(\mathbf{x})$.

Equivalently, one could also keep the angle of incidence fixed and move the aperture. However, the advantage of changing the angle of incidence is that it can be accomplished by using a LED matrix illumination module [27], which means that a conventional microscope can easily be adapted for Fourier ptychography, and that no mechanically moving components need to be introduced. Also, it should be noted that the equivalence only holds when the sample is sufficiently thin so that the object's transmission function is the same for each angle of illumination, and the transmitted wave can be approximated by a simple multiplication. For thick samples where the approximation is not valid, the portion of the 3D Fourier transform of the object that is reconstructed depends on whether the aperture is shifted whether the incident angle of the illumination is varied [28] (also see Section 4.4.2).

4 Extensions

So far, we have discussed variations of the ptychographical algorithm, which are obtained by viewing the phase retrieval problem from different perspectives and using different approaches to solve the problem. These variations differ in certain properties such as their convergence behavior, noise robustness, and required computational power, but they all solve the same basic problem. That is, in all cases, we need to assume for example the following:

- The probe function $P(\mathbf{x})$ is known precisely.
- The probe positions $\mathbf{X}_j$ are known precisely.
- The light is coherent so that the far-field propagation can be modeled with a single Fourier transform.
- The object is sufficiently thin so that the exit waves $\psi_j(\mathbf{x})$ can be calculated using a simple multiplication $O(\mathbf{x})P(\mathbf{x}-\mathbf{X}_j)$.

What we will discuss next are variations of ptychographical algorithms that aim to deal with scenarios where some of the aforementioned assumptions do not hold. In this article, the extensions are presented separately for the sake of a clearer structure, but of course, it is possible to combine them. For example, one can retrieve the object,

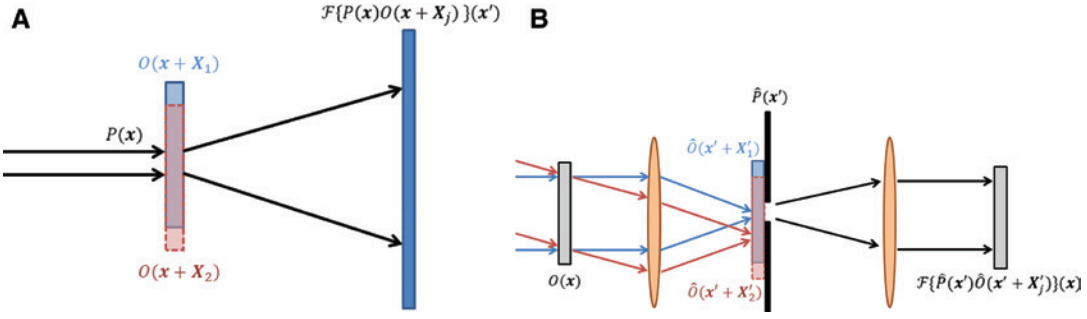

Figure 6: Left: In regular ptychography, the object $O(\mathbf{x})$ is shifted with respect to the probe, and with the corresponding intensity measurements, $O(\mathbf{x})$ can be reconstructed with a ptychographic algorithm. Right: In Fourier ptychography, the object $O(\mathbf{x})$ is illuminated with plane waves from different angles so that the Fourier transform $\hat{O}(\mathbf{x}')$ is shifted with respect to an aperture. Using a ptychographic algorithm, $\hat{O}(\mathbf{x}')$ is reconstructed, which can be inverse Fourier transformed to find $O(\mathbf{x})$. (A) Regular ptychography. (B) Fourier ptychography.

probe, and probe positions at the same time for partially coherent illumination. Also, even though simultaneous retrieval of both object and probe is, here, presented simply as an extension of PIE (as it happened chronologically), it should be noted that this is a crucial part of ptychography and was, in large part, responsible for its success.

4.1 Probe retrieval: ePIE

In the previous algorithms, we assumed that the probe $P(\mathbf{x})$ is known, the object $O(\mathbf{x})$ is unknown, and that the probe is shifted to known positions $\mathbf{X}_j$. However, if we consider far-field propagation, we could also keep the probe stationary and shift the object by $-\mathbf{X}_j$ to get the same intensity patterns

$$\begin{aligned}|\Psi(\mathbf{x}')|^2 &= |\mathcal{F}\{O(\mathbf{x})P(\mathbf{x}-\mathbf{X}_j)\}|^2 \\ &= |\mathcal{F}\{O(\mathbf{x}+\mathbf{X}_j)P(\mathbf{x})\}|^2 .\end{aligned} \tag{32}$$

Thus, the same scheme that we used to update an object estimate if the probe is known, we can also use to update a probe estimate if the object is known. Even though we assumed far-field propagation to obtain this symmetry, it should be stressed that this is just to understand the ePIE update scheme more intuitively, and it does not mean that probe retrieval is not possible in the case of near-field ptychography [29, 30]. If both probe and object are not precisely known, we can assume that the estimates for the probe and object we have are accurate enough to update the estimate for the object and probe, respectively [21, 22, 31]. For example, when using the steepest-descent scheme with incremental updates

$$\begin{aligned}O_k(\mathbf{x}) &:= O_k(\mathbf{x}) - \mu P_k(\mathbf{x}-\mathbf{X}_j)^*(f_{O,k,j}(\mathbf{x}) - f^{\text{upd}}_{O,k,j}(\mathbf{x})), \\ P_k(\mathbf{x}) &:= P_k(\mathbf{x}) - \mu O_k(\mathbf{x}+\mathbf{X}_j)^*(f_{P,k,j}(\mathbf{x}) - f^{\text{upd}}_{P,k,j}(\mathbf{x})),\end{aligned} \tag{33}$$

where

$f_{O,k,j}(\mathbf{x}) = O(\mathbf{x})P(\mathbf{x}-\mathbf{X}_j)$ is the k^{th} estimate of the exit wave for a shifted probe,
$f_{P,k,j}(\mathbf{x}) = O(\mathbf{x}+\mathbf{X}_j)P(\mathbf{x}) = f_{O,k,j}(\mathbf{x}+\mathbf{X}_j)$ is the k^{th} estimate of the exit wave for a shifted object,
$F_{O,k,j}(\mathbf{x}') = \mathcal{F}\{f_{O,k,j}(\mathbf{x})\}(\mathbf{x}')$ is the estimated diffracted field for a shifted probe,
$F_{P,k,j}(\mathbf{x}') = \mathcal{F}\{f_{P,k,j}(\mathbf{x})\}(\mathbf{x}')$ is the estimated diffracted field for a shifted object,
$f^{\text{upd}}_{O,k,j}(\mathbf{x}) = \mathcal{F}^{-1}\left\{\frac{|\Psi(\mathbf{x}')|}{|F_{O,k,j}(\mathbf{x}')|}F_{O,k,j}(\mathbf{x}')\right\}$ is the updated estimated diffracted field for a shifted probe,
$f^{\text{upd}}_{P,k,j}(\mathbf{x}) = \mathcal{F}^{-1}\left\{\frac{|\Psi(\mathbf{x}')|}{|F_{P,k,j}(\mathbf{x}')|}F_{P,k,j}(\mathbf{x}')\right\} = f^{\text{upd}}_{O,k,j}(\mathbf{x}+\mathbf{X}_j)$ is the updated estimated diffracted field for a shifted object. (34)

and k gets increased to $k+1$ when the update has been applied for all positions $\mathbf{X}_j$. Note that due to the simple relation between $f^{\text{upd}}_{P,k,j}(\mathbf{x})$ and $f^{\text{upd}}_{O,k,j}(\mathbf{x})$, one does not need to perform extra fast Fourier transforms (FFTs) to compute $f^{\text{upd}}_{P,k,j}(\mathbf{x})$, which would be computationally expensive. What this means is that if the probe contains unknown aberrations, the algorithm can reconstruct the correct probe so that the quality of the object reconstruction is not degraded by an incorrect probe estimate. However, when using the steepest-descent method, the initial estimate of the probe and/or object should be sufficiently accurate because, otherwise, the estimates cannot be updated reliably, and the algorithm will diverge. To remedy this problem, one can use more sophisticated update schemes such as the DM to ensure initial convergence and use the steepest-descent scheme for final refinement [21].

4.2 Probe position correction

Let us assume that we know $P(\mathbf{x})$, that $P(\mathbf{x})$ has a finite support, and that there is some uncertainty in the probe positions $\mathbf{X}_j$. In principle, one could use a single-intensity phase retrieval algorithm such as HIO to reconstruct the exit waves $\psi_j(\mathbf{x})$ for each probe position separately, calculate the object $O(\mathbf{x}) \approx \frac{P(\mathbf{x})^*\psi_j(\mathbf{x})}{|P(\mathbf{x})|^2+\alpha}$ for each probe position, and from these object reconstructions, one could infer the positions $\mathbf{X}_j$ by seeing where these reconstruction overlap. This can be determined by seeing where the cross-correlation of two reconstructions at adjacent positions attains its maximum. This procedure defeats a bit the purpose of doing ptychography though, as the point of ptychography is to use the overlap between adjacent probes during the reconstruction to make the algorithm more robust. However, it does illustrate the notion that one should be able to correct for any errors in the

probe positions. In order to reconstruct the probe positions while still benefiting from the robustness provided by the overlap between probes, an update scheme is required that updates the object (and probe, if it contains any uncertainties) and probe positions simultaneously. Several such update schemes are discussed in the following. In these methods, one is sometimes required to shift functions by an amount that does not correspond to an integer number of pixels. To perform these subpixel shifts, one can Fourier transform the function, multiply it with a linear phase function, and inverse Fourier transform it [13].

4.2.1 Cost function minimization

Let us write the probe positions as $\mathbf{X}_j = [X_j, Y_j]$. We have seen how we can use a gradient-descent method to minimize a cost function L to optimize the object reconstruction $O(\mathbf{x})$ and probe reconstruction $P(\mathbf{x})$. Similarly, we could consider the probe positions X_j, Y_j as optimization variables and calculate $\frac{\partial L}{\partial X_j}$, $\frac{\partial L}{\partial Y_j}$ to employ a gradient descent scheme

$$X_{j,k+1} = X_{j,k} - \mu \frac{\partial L}{\partial X_{j,k}},$$
$$Y_{j,k+1} = Y_{j,k} - \mu \frac{\partial L}{\partial Y_{j,k}}, \tag{35}$$

though a gradient descent tends to get trapped in local minima quite easily. It was demonstrated in Ref. [22] that a conjugate gradient scheme to update the object, probe, and probe positions simultaneously can correct for small errors in the probe positions. In Ref. [32], it is proposed to use ePIE or DM to update the object and probe functions, while using a conjugate gradient update scheme to update the probe positions. In Ref. [33], Powell's conjugate direction method is used to update the probe positions. The step size of the update can be chosen to be a fixed small constant, or it can be found by performing a line search [32]. Other methods to decide on the step size of a certain update scheme are to start with a certain value and decrease it linearly to a small or zero value over a set number of iterations [34], or to decrease the step size once the direction in which the probe positions are being updated starts oscillating [35]. Note that of these methods, performing a line search is more computationally demanding as it requires performing additional FFTs. Another method to correct errors in the probe positions is to assume a drift model that parameterizes the probe positions, so that the cost function that needs to be minimized depends on fewer optimization variables, which allows one to find its global minimum by trial and error [36].

4.2.2 Annealing

Given probe position estimates $\mathbf{X}_{j,k}$, we can create a set of $M+1$ estimated probe positions consisting of the original estimate $\mathbf{X}_{j,k}$ and M randomly perturbed probe positions [34]

$$\mathbf{X}^{\text{pert}}_{j,k,0} = \mathbf{X}_{j,k}$$
$$\mathbf{X}^{\text{pert}}_{j,k,m} = \mathbf{X}_{j,k} + \mathbf{C}_m \quad m = 1 \ldots M. \tag{36}$$

Here, $\mathbf{C}_m$ are vectors $[c_x, c_y]$ where c_x, c_y are randomly drawn from some interval $[-c, c]$. The parameter c can be chosen to be smaller as the algorithm progresses so that the correct probe positions can be found more accurately. For all M perturbed probe positions $\mathbf{X}^{\text{pert}}_{j,k,m}$, one can calculate the error between the estimated and the measured amplitude pattern

$$E_{j,m} = \sum_{\mathbf{x}'} (|F_{j,k,m}(\mathbf{x}')| - |\Psi_j(\mathbf{x}')|)^2, \tag{37}$$

where

$$F_{j,k,m}(\mathbf{x}') = \mathcal{F}\{O(\mathbf{x}) P(\mathbf{x} - \mathbf{X}^{\text{pert}}_{j,k,m})\}(\mathbf{x}'). \tag{38}$$

Let $\mathbf{X}^{\text{pert}}_{j,k,n}$ be the probe position for which this error $E_{j,n}$ is minimal. We apply an ePIE update (or an update of some other object reconstruction scheme) to the object and the probe using this probe position, and we choose it to be our next estimated probe position

$$\mathbf{X}_{j,k+1} = \mathbf{X}^{\text{pert}}_{j,k,n}. \tag{39}$$

Note that for each $\mathbf{C}_m$, one has to perform an additional FFT, which increases the computational demands of the algorithm. A similar annealing method has been used for Fourier ptychography [37].

4.2.3 Cross-correlation

The cross-correlation method [35] is based on the observation that if one applies to $O_k(\mathbf{x})$, an ePIE update for an estimated probe position $\mathbf{X}_{j,k}$, the updated object estimate $O^{\text{upd},j}_k(\mathbf{x})$ is shifted toward the true position

$\mathbf{X}_j$. This shift $\mathbf{C}_{j,k}$ is used to update the estimated probe position

$$\mathbf{X}_{i.k+1} = \mathbf{X}_{i.k} + \mu \mathbf{C}_{i.k}, \tag{40}$$

where μ is an update parameter. To find the shift $\mathbf{C}_{j,k}$, one can find the peak of the cross-correlation of $O_k^{\mathrm{upd},j}(\mathbf{x})\Pi_k(\mathbf{x}-\mathbf{X}_{k,j})$ and $O_k(\mathbf{x})\Pi_k(\mathbf{x}-\mathbf{X}_{k,j})$. Here, $\Pi_k(\mathbf{x}-\mathbf{X}_{k,j})$ is a step function that indicates the region where the probe has a sufficiently strong amplitude:

$$\Pi_k(\mathbf{x}) = \begin{cases} 1 & \text{if } \dfrac{|P_k(\mathbf{x})|}{\max_{\mathbf{x}}|P_k(\mathbf{x})|} > \alpha, \\ 0 & \text{otherwise,} \end{cases} \tag{41}$$

where α is a threshold value. The computationally expensive step in this method is to perform the FFTs required to compute the cross-correlation function and to find the location of its maximum with subpixel accuracy [38].

4.2.4 Intensity gradient

If we assume that we have sufficiently good estimates of the probe and the object, and that the difference between the estimated intensity pattern

$$|F_{k,j}(\mathbf{x}')|^2 = |\mathcal{F}\{O_k(\mathbf{x})P_k(\mathbf{x}-\mathbf{X}_{j,k})\}(\mathbf{x}')|^2 \tag{42}$$

and the measured intensity pattern $|\Psi_j(\mathbf{x}')|^2$ is mainly due to an error

$$\Delta\mathbf{X}_{j,k} = [\Delta X_{j,k}, \Delta Y_{j,k}] \tag{43}$$

in the estimated probe position

$$\mathbf{X}_{j,k} = [X_{j,k}, Y_{j,k}]. \tag{44}$$

Then, we can write

$$|\Psi_j(\mathbf{x}')|^2 \approx |\mathcal{F}\{O_k(\mathbf{x})P_k(\mathbf{x}-(\mathbf{X}_{j,k}+\Delta\mathbf{X}_{j,k}))\}(\mathbf{x}')|^2 . \tag{45}$$

We can linearize the difference between the estimated and measured intensity as

$$|\Psi_j(\mathbf{x}')|^2 - |F_{k,j}(\mathbf{x}')|^2 \approx \frac{\partial|F_{k,j}(\mathbf{x}')|^2}{\partial X_{j,k}}\Delta X_{j,k} + \frac{\partial|F_{k,j}(\mathbf{x}')|^2}{\partial Y_{j,k}}\Delta Y_{j,k}. \tag{46}$$

In this equation, we can calculate the derivatives of $|F_{k,j}(\mathbf{x}')|^2$ numerically, so the only unknowns are $\Delta X_{j,k}$ and $\Delta Y_{j,k}$. We can write this equation as a matrix-vector equation

$$u = Av, \tag{47}$$

where

$$u = \begin{bmatrix} |\Psi_j(\mathbf{x}'_1)|^2 - |F_{k,j}(\mathbf{x}'_1)|^2 \\ \vdots \\ |\Psi_j(\mathbf{x}'_N)|^2 - |F_{k,j}(\mathbf{x}'_N)|^2 \end{bmatrix},$$

$$A = \begin{bmatrix} \dfrac{\partial|F_{k,j}(\mathbf{x}'_1)|^2}{\partial X_{j,k}} & \dfrac{\partial|F_{k,j}(\mathbf{x}'_1)|^2}{\partial Y_{j,k}} \\ \vdots & \vdots \\ \dfrac{\partial|F_{k,j}(\mathbf{x}'_N)|^2}{\partial X_{j,k}} & \dfrac{\partial|F_{k,j}(\mathbf{x}'_N)|^2}{\partial Y_{j,k}} \end{bmatrix}, \quad v = \begin{bmatrix} \Delta X_{j,k} \\ \Delta Y_{j,k} \end{bmatrix}, \tag{48}$$

where N is the number of pixels on the detector. One can find the least-squares solution for v using

$$v_{\mathrm{LS}} = (A^T A)^{-1} A^T u, \tag{49}$$

where it should be noted that A^TA is a 2×2 matrix, so its inversion is computationally inexpensive. The estimated probe positions are then updated as [39]

$$\begin{aligned} X_{j,k+1} &= X_{j,k} + \mu\Delta X_{j,k}, \\ Y_{j,k+1} &= Y_{j,k} + \mu\Delta Y_{j,k}, \end{aligned} \tag{50}$$

where μ is an update parameter. The computationally expensive step lies in computing the matrix A, which requires four FFTs to numerically calculate the derivatives

$$\frac{\partial|F_{k,j}(\mathbf{x}')|^2}{\partial X_{j,k}} \approx \frac{|\mathcal{F}\{O_k(\mathbf{x})P_k(\mathbf{x}-(\mathbf{X}_{j,k}+d\mathbf{X}))\}(\mathbf{x}')|^2 - |\mathcal{F}\{O_k(\mathbf{x})P_k(\mathbf{x}-\mathbf{X}_{j,k})\}(\mathbf{x}')|^2}{|d\mathbf{X}|}, \tag{51}$$

but it should be remarked that $\mathcal{F}\{O_k(\mathbf{x})P_k(\mathbf{x}-\mathbf{X}_{j,k})\}(\mathbf{x}')$ needs to be calculated anyway to perform the object update (e.g. using ePIE).

4.2.5 Direct estimation

Almost all the methods that have been discussed so far relied on using an iterative algorithm to incrementally improve the probe position estimates while simultaneously reconstructing the object and probe. However, there are also methods that can infer good estimates for the probe positions more or less directly from the measured intensity patterns. For example, shadow images, Gabor holography [40] and Fourier holography [41], have been used to directly obtain a decent reconstruction of the exit

wave from its diffraction pattern. The reconstructions at adjacent probe positions are then used to calculate the displacement between the probe positions using a cross-correlation method. Another method is to use a setup where the measured diffraction pattern is the image of a pinhole that is perturbed by a weakly scattering sample [42]. To shift the probe to another probe position, the pinhole is shifted, and therefore, the image of the pinhole is shifted proportionally. This way, one can infer the probe positions directly from the measured intensity patterns.

4.3 Partial coherence

When the incident field is partially coherent (either spatially or temporally), one cannot describe the transmitted exit wave simply as $\psi_j(\mathbf{x})$, or the diffracted field as $\Psi(\mathbf{x}')$. Instead, we can decompose the illuminating field into modes and reconstruct them separately. If the incident field is spatially partially coherent, and if the coherence of two points depends only on the difference between them, then, the diffracted intensity patterns can be described as a convolution of a completely coherent diffracted intensity pattern with the Fourier transform of the degree of coherence function. Whether using spatially partially coherent illumination can benefit the reconstruction quality has been discussed in Refs. [14] and [43]. In the following, we describe in more detail how the ptychographic algorithm can be adapted to deal with partial coherence.

4.3.1 Mode decomposition

Let us denote the incident field as $U(\mathbf{x}, t)$, and let us assume that it is quasi-monochromatic with frequency ω so that we can write

$$U(\mathbf{x}, t) = P(\mathbf{x}, t)e^{-i\omega t}. \tag{52}$$

The incident field has a mutual intensity $J(\mathbf{x}_1, \mathbf{x}_2)$ that describes the correlation of a quasi-monochromatic field $P(\mathbf{x}, t)$ between pairs of points $(\mathbf{x}_1, \mathbf{x}_2)$

$$\begin{aligned} J(\mathbf{x}_1, \mathbf{x}_2) &= \langle U(\mathbf{x}_1, t)^* U(\mathbf{x}_2, t)\rangle \\ &= \langle P(\mathbf{x}_1, t)^* P(\mathbf{x}_2, t)\rangle, \end{aligned} \tag{53}$$

where the brackets denote the time-average. From Mercer's theorem, it follows that we can decompose the partially coherent field in coherent modes [44, 45]

$$J(\mathbf{x}_1, \mathbf{x}_2) = \sum_n P_n(\mathbf{x}_1)^* P_n(\mathbf{x}_2). \tag{54}$$

Defining $\psi_n(\mathbf{x}) = O(\mathbf{x})P_n(\mathbf{x})$, the far-field intensity is given by

$$\begin{aligned} I(\mathbf{x}') &= \iint J(\mathbf{x}_1, \mathbf{x}_2) O(\mathbf{x}_1)^* O(\mathbf{x}_2) e^{-2\pi i(\mathbf{x}_2 - \mathbf{x}_1)\cdot\mathbf{x}'} \mathrm{d}\mathbf{x}_1 \mathrm{d}\mathbf{x}_2 \\ &= \sum_n \left| \int \psi_n(\mathbf{x}) e^{-2\pi i \mathbf{x}\cdot\mathbf{x}'} \mathrm{d}\mathbf{x} \right|^2 \\ &= \sum_n |\Psi_n(\mathbf{x}')|^2 . \end{aligned} \tag{55}$$

So the intensity is found by writing the incident partially coherent field as multiple coherent modes that are mutually incoherent, propagating each mode coherently, and adding the diffracted intensities incoherently. Technically, there are, in general, an infinite number of modes required to describe the partially coherent field, but in practice, only a finite number of modes are necessary to describe the field with sufficient accuracy. The more coherent the field is, the fewer modes are required, and if the field is fully coherent, only one mode is required. The same procedure can be applied when the incident field is temporally partially coherent (i.e. when it consists of multiple wavelengths), in which case each mode corresponds to a certain wavelength. Also, when multiple wavelengths are considered, it is possible that the object responds differently to each wavelength, and therefore, one would also have to introduce different object modes $O_n(\mathbf{x})$. For the ptychographical algorithm, this means that instead of just one exit wave $\psi(\mathbf{x})$, we have to reconstruct several modes $\psi_n(\mathbf{x})$. We define the cost functional

$$L = \sum_{\mathbf{x}'} \left(\sqrt{\sum_n |F_n(\mathbf{x}')|^2} - \sqrt{I(\mathbf{x}')} \right)^2 . \tag{56}$$

In the case of using multiple wavelengths where each illumination mode $P_n(\mathbf{x})$ is associated with a separate object mode $O_n(\mathbf{x})$, we can update the estimates as [46]

$$\begin{aligned} O_{n,k}(\mathbf{x}) &:= O_{n,k}(\mathbf{x}) - \mu \frac{\partial L}{\partial O_{n,k}(\mathbf{x})^*}, \\ P_{n,k}(\mathbf{x}) &:= P_{n,k}(\mathbf{x}) - \mu \frac{\partial L}{\partial P_{n,k}(\mathbf{x})^*}. \end{aligned} \tag{57}$$

The derivatives can be calculated to be

$$\begin{aligned} \frac{\partial L}{\partial O_{n,k}(\mathbf{x})^*} &= P_{n,k}(\mathbf{x} - \mathbf{X}_j)^* (f_{O,k,j,n}(\mathbf{x}) - f^{\mathrm{upd}}_{O,k,j,n}(\mathbf{x})), \\ \frac{\partial L}{\partial P_{n,k}(\mathbf{x})^*} &= O_{n,k}(\mathbf{x} + \mathbf{X}_j)^* (f_{P,k,j,n}(\mathbf{x}) - f^{\mathrm{upd}}_{P,k,j,n}(\mathbf{x})), \end{aligned} \tag{58}$$

where

$$
\begin{aligned}
&f_{O,k,j,n}(\mathbf{x}) = O_{n,k}(\mathbf{x})P_{n,k}(\mathbf{x}-\mathbf{X}_j) \text{ is the } k^{\text{th}} \text{ estimate of the } n^{\text{th}} \text{ mode of the exit wave for a shifted probe,}\\
&f_{P,k,j,n}(\mathbf{x}) = O_{n,k}(\mathbf{x}+\mathbf{X}_j)P_{n,k}(\mathbf{x}) \text{ is the } k^{\text{th}} \text{ estimate of the } n^{\text{th}} \text{ mode of the exit wave for a shifted object,}\\
&F_{O,k,j,n}(\mathbf{x}') = \mathcal{F}\{f_{O,k,j,n}(\mathbf{x})\}(\mathbf{x}') \text{ is the estimated diffracted field for a shifted probe,}\\
&F_{P,k,j,n}(\mathbf{x}') = \mathcal{F}\{f_{P,k,j,n}(\mathbf{x})\}(\mathbf{x}') \text{ is the estimated diffracted field for a shifted object,}\\
&f^{\text{upd}}_{O,k,j,n}(\mathbf{x}) = \mathcal{F}^{-1}\left\{\frac{\sqrt{I(\mathbf{x}')}}{\sqrt{\sum_n |F_{O,k,j,n}(\mathbf{x}')|^2}}F_{O,k,j,n}(\mathbf{x}')\right\} \text{ is the updated estimated diffracted field for a shifted probe,}\\
&f^{\text{upd}}_{P,k,j,n}(\mathbf{x}) = \mathcal{F}^{-1}\left\{\frac{\sqrt{I(\mathbf{x}')}}{\sqrt{\sum_n |F_{P,k,j,n}(\mathbf{x}')|^2}}F_{P,k,j,n}(\mathbf{x}')\right\} \text{ is the updated estimated diffracted field for a shifted object.}
\end{aligned}
\tag{59}
$$

Like in Eq. (34), it should be noted that because of the simple relation between updated exit waves, no additional Fourier transform needs to be performed. In the case of a quasi-monochromatic spatially partially coherent illumination where each illumination mode $P_n(\mathbf{x})$ sees the same object $O(\mathbf{x})$, the update for the object estimate is slightly different [14]

$$
\begin{aligned}
&O_{k+1}(\mathbf{x}) = O_k(\mathbf{x}) - \mu\frac{\partial L}{\partial O_k(\mathbf{x})^*},\\
&\frac{\partial L}{\partial O(\mathbf{x})^*} = \sum_n P_n(\mathbf{x}-\mathbf{X}_j)^*(f_{O,k,j,n}(\mathbf{x}) - f^{\text{upd}}_{O,k,j,n}(\mathbf{x})),
\end{aligned}
\tag{60}
$$

where $f_{O,k,j,n}(\mathbf{x}) = O_k(\mathbf{x})P_{n,k}(\mathbf{x}-\mathbf{X}_j)$.

4.3.2 Convolution

If we define $P(\mathbf{x}) = \langle P(\mathbf{x}, t)\rangle$ (where $P(\mathbf{x}, t)$ is defined in Eq. (52)), then, we can define the degree of coherence as

$$
\gamma(\mathbf{x}_1, \mathbf{x}_2) = \frac{\langle P(\mathbf{x}_1, t)^* P(\mathbf{x}_2, t)\rangle}{P(\mathbf{x}_1)^* P(\mathbf{x}_2)},
\tag{61}
$$

so that $J(\mathbf{x}_1, \mathbf{x}_2) = P(\mathbf{x}_1)^* P(\mathbf{x}_2)\gamma(\mathbf{x}_1, \mathbf{x}_2)$. In case we assume that $\gamma(\mathbf{x}_1, \mathbf{x}_2)$ only depends on the difference between the two points $\mathbf{x}_1$, $\mathbf{x}_2$, i.e. $\gamma(\mathbf{x}_1, \mathbf{x}_2) = \gamma(0, \mathbf{x}_2 - \mathbf{x}_1)$, we can write the far-field intensity as a convolution, and the ptychographic algorithm can be changed accordingly. To demonstrate this, we inverse Fourier transform $I(\mathbf{x}')$, giving

$$
\begin{aligned}
\mathcal{F}^{-1}\{I(\mathbf{x}')\}(\mathbf{x}) &= \iiint \gamma(\mathbf{x}_1, \mathbf{x}_2)P(\mathbf{x}_1)^* P(\mathbf{x}_2)O(\mathbf{x}_1)^* O(\mathbf{x}_2)e^{-2\pi i(\mathbf{x}_2-\mathbf{x}_1)\cdot\mathbf{x}'}e^{2\pi i\mathbf{x}\cdot\mathbf{x}'}\,\mathrm{d}\mathbf{x}_1\,\mathrm{d}\mathbf{x}_2\,\mathrm{d}\mathbf{x}'\\
&= \iint \gamma(\mathbf{x}_1, \mathbf{x}_1+\mathbf{x})P(\mathbf{x}_1)^* O(\mathbf{x}_1)^* P(\mathbf{x}_1+\mathbf{x})O(\mathbf{x}_1+\mathbf{x})\mathrm{d}\mathbf{x}_1\\
&= \gamma(\mathbf{0}, \mathbf{x})\iint \psi(\mathbf{x}_1)^*\psi(\mathbf{x}_1+\mathbf{x})\mathrm{d}\mathbf{x}_1\\
&= \mathcal{F}^{-1}\{\Gamma(\mathbf{x}')\}(\mathbf{x})\mathcal{F}^{-1}\{|\Psi(\mathbf{x}')|^2\}(\mathbf{x}),
\end{aligned}
\tag{62}
$$

where $\Gamma(\mathbf{x}')$ denotes the Fourier transform of $\gamma(\mathbf{x}, \mathbf{0})$, and $|\Psi(\mathbf{x}')|^2$ denotes the diffraction pattern if the incident field is coherent. By Fourier transforming this back to diffraction space, we get a convolution [47, 48]

$$
I(\mathbf{x}') = \Gamma(\mathbf{x}') \otimes |\Psi(\mathbf{x}')|^2 .
\tag{63}
$$

So we see that $\Gamma(\mathbf{x}')$ acts as a sort of point spread function that blurs the diffraction pattern more as the incident light becomes less coherent. The modulus constraint projection is

$$
f^{\text{upd}}_k(\mathbf{x}) = \mathcal{F}^{-1}\left\{F_k(\mathbf{x}')\frac{\sqrt{I(\mathbf{x}')}}{\sqrt{\Gamma(\mathbf{x}')\otimes|F_k(\mathbf{x}')|^2}}\right\}.
\tag{64}
$$

In case $\Gamma(\mathbf{x}')$ is unknown, it has been suggested that it can be updated during the iterative algorithm by employing a Richardson-Lucy algorithm [48] or by minimizing a cost functional such as

$$
L = \sum_{\mathbf{x}'}(I(\mathbf{x}') - \Gamma(\mathbf{x}')\otimes|F_k(\mathbf{x}')|^2)^2
\tag{65}
$$

with respect to $\Gamma(\mathbf{x}')$ [47].

4.4 3D Objects

So far, we have assumed that the exit wave can be computed by simply multiplying the incident illumination with the object transmission function $\psi(\mathbf{x}) = P(\mathbf{x})O(\mathbf{x})$. However, this is an approximation that holds only for thin samples. In the following, we discuss ptychographic

algorithms that reconstruct thicker samples for which the multiplicative approximation does not hold.

4.4.1 Multislice method

In the multislice method [49], the object is modeled as a sequence of N slices O_n separated by some distance Δ_z (it does not necessarily have to be a fixed distance, but for simplicity, let us assume in this case it is). For each slice, we assume the multiplicative approximation holds, and we assume that in between the slices, the light propagates freely. Thus, if we define $\mathcal{P}_{\Delta_z}$ to be the propagator (e.g. the angular spectrum propagator) over a distance Δ_z, we can model the forward calculation as

$$\Psi_j(\mathbf{x}') = \mathcal{F}\{O_N(\mathbf{x})\mathcal{P}_{\Delta_z} O_{N-1}(\mathbf{x})\mathcal{P}_{\Delta_z} \dots O_2(\mathbf{x})\mathcal{P}_{\Delta_z} O_1(\mathbf{x})P(\mathbf{x}-\mathbf{X}_j)\}. \tag{66}$$

At the n^{th} slice, we can define the incident wave as

$$P_{j,n}(\mathbf{x}) = \mathcal{P}_{\Delta_z} O_{n-1}(\mathbf{x})\mathcal{P}_{\Delta_z} \dots O_2(\mathbf{x})\mathcal{P}_{\Delta_z} O_1(\mathbf{x})P(\mathbf{x}-\mathbf{X}_j), \tag{67}$$

with

$$P_{j,1}(\mathbf{x}) = P(\mathbf{x}-\mathbf{X}_j), \tag{68}$$

and we define the exit wave as

$$\psi_{j,n}(\mathbf{x}) = P_{j,n}(\mathbf{x})O_n(\mathbf{x}). \tag{69}$$

This is illustrated in Figure 7. Given the object estimates $O_{n,k}(\mathbf{x})$ and probe estimate $P_k(\mathbf{x})$, we can use Eq. (66) to calculate the estimated intensity pattern $|F_{j,k}(\mathbf{x}')|^2$; we can use the measured intensity pattern $|\Psi_j(\mathbf{x}')|^2$ to update the estimated field $F_{j,k}(\mathbf{x}')$ as

$$F_{j,k}^{\text{upd}}(\mathbf{x}') = \frac{F_{j,k}(\mathbf{x}')}{|F_{j,k}(\mathbf{x}')|}|\Psi_j(\mathbf{x}')|. \tag{70}$$

We can propagate this updated field back through all the slices from $n=N$ to $n=0$ and use ePIE iterations to update each incident wave estimate $P_{j,n,k}(\mathbf{x})$ and object estimate $O_{n,k}(\mathbf{x})$ using the estimated exit waves $f_{j,n,k}(\mathbf{x}) = P_{j,n,k}(\mathbf{x})O_{n,k}(\mathbf{x})$

$$\begin{aligned} O_{n,k+1}(\mathbf{x}) &= O_{n,k}(\mathbf{x}) + \mu P_{j,n,k}(\mathbf{x})^*(f_{j,n,k}^{\text{upd}}(\mathbf{x}) - f_{j,n,k}(\mathbf{x})) \\ P_{j,n,k+1}(\mathbf{x}) &= P_{j,n,k}(\mathbf{x}) + \mu O_{n,k}(\mathbf{x})^*(f_{j,n,k}^{\text{upd}}(\mathbf{x}) - f_{j,n,k}(\mathbf{x})) \end{aligned} \tag{71}$$

where

$$\begin{aligned} f_{j,N,k}^{\text{upd}}(\mathbf{x}) &= \mathcal{F}^{-1}\{F_{j,k}^{\text{upd}}(\mathbf{x}')\}(\mathbf{x}), \\ f_{j,n,k}^{\text{upd}}(\mathbf{x}) &= \mathcal{P}_{-\Delta_z} P_{j,n+1,k+1}. \end{aligned} \tag{72}$$

This method has been termed 3PIE [49]. Another approach, where the update of the slices is applied simultaneously rather than sequentially, is described in Ref. [50]. In order for this procedure to work, one should take care that the slices are sufficiently far apart so that the multiplicative approximation cannot be applied to two consecutive slices because, otherwise, there would be no unique solution for $O_n(\mathbf{x})$ and $O_{n+1}(\mathbf{x})$: $g(\mathbf{x})O_n(\mathbf{x})$ and $\frac{1}{g(\mathbf{x})}O_{n+1}(\mathbf{x})$ would then be solutions as well for arbitrary $g(\mathbf{x})$. However, at the same time, the slices should be sufficiently close so that for each single slice, the multiplicative approximation holds. Also, it should be noted that if each slice $O_n(\mathbf{x})$ is multiplied by some constant c_n such that $\Pi_n c_n = 1$, the same diffraction pattern is obtained, thus, leading to multiple solutions. An advantage of this method is that multiple scattering is taken into account by propagating the field that is scattered by each slice.

An extension of this method has been proposed where this procedure is performed for multiple orientations of the sample [51]. If the tilt of the sample is small, one can make the approximation that each slice is translated, as shown in Figure 8. By doing this, a higher resolution in the axial direction can be obtained.

4.4.2 3D Fourier ptychography

A sample is illuminated by plane waves from different angles sequentially. In the case of a 2D sample, changing

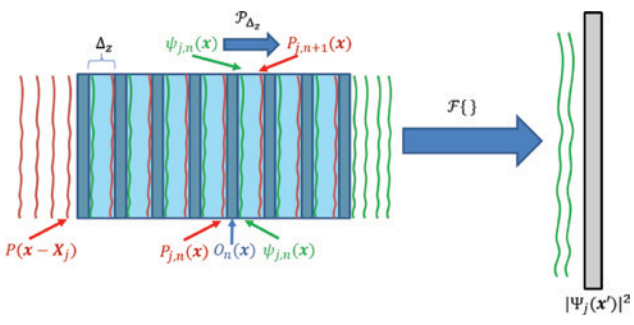

Figure 7: In multislice ptychography, a thick sample is divided in slices, and each slice is reconstructed separately.

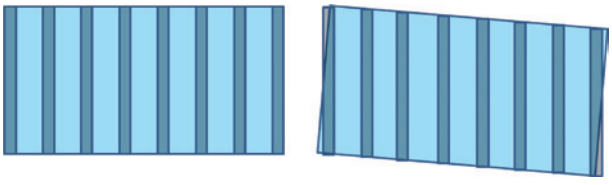

Figure 8: In precession multislice ptychography, a thick sample is tilted to different angles. For small tilt angles, one can make the approximation that each slice is translated.

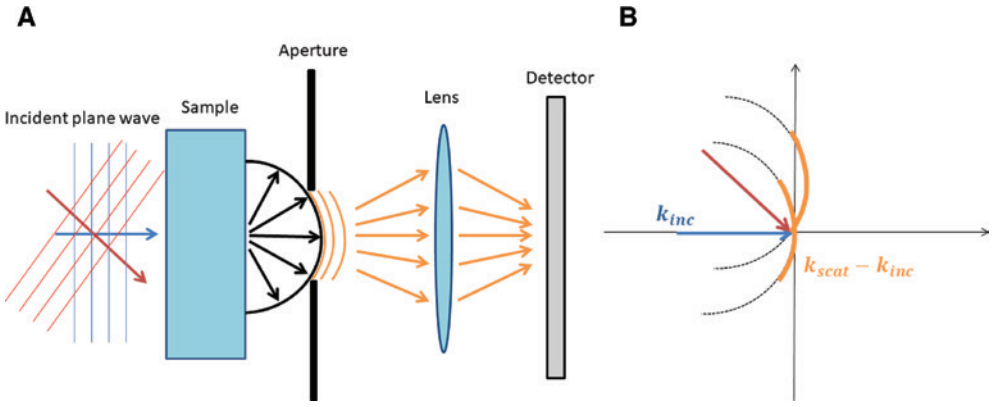

Figure 9: In diffraction Fourier ptychography, a thick sample is illuminated by plane waves from different angles. For each angle, the diffracted transmitted field corresponds to a shell of the Fourier transform of the sample, assuming that the single-scattering approximation holds. By reconstructing these shells, a portion of the Fourier transform of the object can be reconstructed, which can be inverse Fourier transformed to find a 3D reconstruction of the object. (A) Experimental setup. (B) Reconstruction in Fourier space.

the incident angle would simply translate the Fourier transform of the transmitted wave as shown in Figure 6, and the aperture would each time capture a different portion of the Fourier transform. In case of a 3D sample, we can apply the Born approximation (i.e. single-scattering approximation) to find that what we measure is a portion of the shell of the 3D Fourier transform of the sample (Figure 9). If we define $v(\mathbf{x})$ to be the 3D scattering potential, we want to reconstruct, $V(\mathbf{x}')$ its 3D Fourier transform, $\mathbf{k}_{\text{scat}}$ a 3D vector with length $\frac{1}{\lambda}$ pointing in a scattering direction, and $\mathbf{k}_{\text{inc}}$ a 3D vector with length $\frac{1}{\lambda}$ pointing to the direction of the incident plane wave, we can write for the scattered far field $U(\mathbf{k}_{\text{scat}})$

$$U(\mathbf{k}_{\text{scat}}) = V(\mathbf{k}_{\text{scat}} - \mathbf{k}_{\text{inc}}). \tag{73}$$

By changing the incident angle of the illumination $\mathbf{k}_{\text{inc}}$, a different portion of the shell is detected. Just like in 2D ptychography, we alternately project between the measured intensity patterns and overlapping probes; in 3D Fourier ptychography, we alternately project between the measured intensity patterns and overlapping shell portions, though it must be noted that there is much less overlap between shell portions due to their 3D nature. With this procedure, a volume of $V(\mathbf{x}')$ is reconstructed, which can be inverse Fourier transformed to find $v(\mathbf{x})$ with a certain resolution [52]. While this method uses the single-scattering approximation, it does not require the arbitrary division into slices like the multislice approach. However, also in Fourier ptychography, it is possible to reconstruct 3D samples using a multislice method [53].

4.5 Others

While we have discussed quite a few variants of the ptychographical algorithm, still many more have been and are being developed. A few of them are listed below:

1. *Floating PIE* [54]: can be used to interpolate or extrapolate intensity measurements. This can be useful when a central beam stop blocks part of the pattern, when the pattern is undersampled [54], or when the pattern is cut off significantly by the finite size of the detector [13]. It works by applying the amplitude constraints only to the points that are measured, while leaving the other points 'floating'.
2. *Single-shot ptychography* [55]: by putting a pinhole array before a focusing lens, and putting the sample out of focus, the sample is illuminated by multiple probes at the same time, while the diffraction patterns are separated in the detection plane so that they can be measured in a single shot.
3. *Fresnel ptychography* [29, 30]: instead of measuring in the far-field (Fraunhofer regime), the measurements are taken in the Fresnel regime.
4. *Through-focus ptychography* [56]: aside from moving the object laterally with respect to the probe, the object is also moved longitudinally. This is related to the method of probe-diverse ptychography, where different probes are used to scan the object [57].
5. *Vectorial ptychography* [58]: ptychography is extended so that an anisotropy map of the sample can be reconstructed.
6. *Ptychography with an unstable probe* [59]: instead of assuming the probe is fixed for all probe positions,

the probe is assumed to vary slightly for different positions due to instability of the light source. This means that for each probe position, a separate probe is updated. To ensure that the probes are still sufficiently similar, the dimensionality of the set probes is reduced at each iteration, ensuring that the principal component of the probes becomes more prominent.

7. *Nonlinear ptychography* [60]: ptychography is used to image nonlinear optical interactions.
8. *Bragg ptychography* [61–64]: coherent diffractive imaging techniques are used to image strain fields in crystalline structures.

5 Conclusion

In this article, we have provided an overview of different ptychographic algorithms. Even though the list that is presented here is far from exhaustive, an understanding of the mathematical theory that underpins the algorithms will help with digesting the current as well as future literature on this topic more easily, and it can help starting researchers generating their own ideas on this topic. Moreover, the examples of the extensions of the ptychographic algorithm should give some impression of what is possible with this technique.

Acknowledgments: The author would like to thank Prof. W.M.J. Coene for discussions on the topic of this manuscript.

References

[1] J. R. Fienup, Opt. Lett. 3, 27 (1978).
[2] J. R. Fienup, Appl. Opt. 21, 2758 (1982).
[3] R. Hunger, Tech. Rep. TUM-LNS-TR-07-06, 2007.
[4] F. Soulez, E. Thiébaut, A. Schutz, A. Ferrari, F. Courbin, et al., Appl. Opt. 55, 7412 (2016).
[5] S. Marchesini, Rev. Sci. Instrum. 78, 11301 (2007).
[6] V. Elser, I. Rankenburg and P. Thibault, Proc. Natl. Acad. Sci. 104, 418–423 (2007).
[7] D. R. Luke, Inverse Probl. 21, 37–50 (2004).
[8] H. H. Bauschke, P. L. Combettes and D. R. Luke, J. Opt. Soc. Am. A, 19, 1334 (2002).
[9] L. Yeh, J. Dong, J. Zhong, L. Tian, M. Chen, et al., Opt. Express 23, 33214 (2015).
[10] L. Bian, J. Suo, J. Chung, X. Ou, C. Yang, et al., Sci. Rep. 6, 27384 (2016).
[11] C. Zuo, J. Sun and Q. Chen, Opt. Express 24, 20724 (2016).
[12] J. Qian, C. Yang, A. Schirotzek, F. Maia and S. Marchesini, Inverse Probl. Appl., Contemp. Math. 615, 261 (2014).
[13] A. M. Maiden, M. J. Humphry, F. Zhang and J. M. Rodenburg, J. Opt. Soc. Am. A 28, 604 (2011).
[14] N. Burdet, K. Shimomura, M. Hirose, A. Suzuki and Y. Takahashi, Appl. Phys. Lett. 108, 071103 (2016).
[15] A. M. Maiden, J. M. Rodenburg and M. J. Humphry, Opt. Lett. 35, 2585 (2010).
[16] A. M. Maiden, G. R. Morrison, B. Kaulich, A. Gianoncelli and J. M. Rodenburg, Nat. Commun. 4, 1669 (2013).
[17] M. Guizar-Sicairos, M. Holler, A. Diaz, J. Vila-Comamala, O. Bunk, et al., Phys. Rev. B 86, 100103(R) (2012).
[18] S. Marchesini, A. Schirotzek, C. Yang, H. Wu and F. Maia, Inverse Probl. 29, 115009 (2013).
[19] C. Wang, Z. Xu, H. Liu, Y. Wang, J. Wang, et al., Appl. Opt. 56, 2099 (2017).
[20] O. Bunk, M. Dierolf, S. Kynde, I. Johnson, O. Marti, et al., Ultramicroscopy 108, 481–487 (2008).
[21] P. Thibault, M. Dierolf, O. Bunk, A. Menzel and F. Pfeiffer, Ultramicroscopy 109, 338–343 (2009).
[22] M. Guizar-Sicairos and J. R. Fienup, Opt. Express 16, 7264 (2008).
[23] P. Thibault and M. Guizar-Sicairos, New J. Phys. 14, 63004 (2012).
[24] A. Maiden, D. Johnson and P. Li, Optica 4, 736 (2017).
[25] S. Ruder, CoRR abs/1609.04747, 2016.
[26] A. P. Konijnenberg, W. M. J. Coene, S. F. Pereira and H. P. Urbach, Ultramicroscopy 171, 43–54 (2016).
[27] G. Zheng, R. Horstmeyer and C. Yang, Nat. Photonics 7, 739 (2013).
[28] P. Li, D. J. Batey, T. B. Edo and J. M. Rodenburg, Ultramicroscopy 158, 1–7 (2015).
[29] D. J. Vine, G. J. Williams, B. Abbey, M. A. Pfeifer, J. N. Clark, et al., Phys. Rev. A 80, 063823 (2009).
[30] M. Stockmar, P. Cloetens, I. Zanette, B. Enders, M. Dierolf, et al., Scientific Reports 3, Article number: 1927 (2013).
[31] A. M. Maiden and J. M. Rodenburg, Ultramicroscopy 109, 1256–1262 (2009).
[32] A. Tripathi, I. McNulty and O. G. Shpyrko, Opt. Express 22, 1452 (2014).
[33] O. Mandula, M. E. Aizarna, J. Eymery, M. Burghammer and V. Favre-Nicolin, J. Appl. Crystallogr. 49, 1842–1848 (2016).
[34] A. M. Maiden, M. J. Humphry, M. C. Sarahan, B. Kraus and J. M. Rodenburg, Ultramicroscopy 120, 64–72 (2012).
[35] F. Zhang, I. Peterson, J. Vila-Comamala, A. Diaz, F. Berenguer, et al., Opt. Express 21, 13592 (2013).
[36] M. Beckers, T. Senkbeil, T. Gorniak, K. Giewekemeyer, T. Salditt, Ultramicroscopy 126(Supplement C), 44–47 (2013).
[37] J. Sun, Q. Chen, Y. Zhang and C. Zuo, Biomed. Opt. Express 7, 1336–1350 (2016).
[38] M. Guizar-Sicairos, S. T. Thurman and J. R. Fienup, Opt. Lett. 33, 156 (2008).
[39] P. Dwivedi, A. P. Konijnenberg, S. F. Pereira and H. P. Urbach, in 'Proceedings Volume 10329, Optical Measurement Systems for Industrial Inspection X; 103292Y', Eds. By P. Lehmann, W. Osten and A. A. Gonçalves (SPIE, 2017).
[40] A. C. Hurst, T. B. Edo, T. Walther, F. Sweeney and J. M. Rodenburg, J. Phys. Conf. Ser. 241, 012004 (2010).
[41] P. Hessing, B. Pfau, E. Guehrs, M. Schneider, L. Shemilt, et al., Opt. Express 24, 1840–1851 (2016).
[42] X. Pan, C. Liu, Q. Lin and J. Zhu, Opt. Express 21, 6162–6168 (2013).
[43] K. Stachnik, I. Mohacsi, I. Vartiainen, N. Stuebe, J. Meyer, et al., Appl. Phys. Lett. 107, 011105 (2015).

[44] E. Wolf, J. Opt. Soc. Am. 72, 343 (1982).
[45] P. Thibault and A. Menzel, Nature 494, 68–71 (2013).
[46] D. J. Batey, D. Claus and J. M. Rodenburg, Ultramicroscopy 138, 13–21 (2014).
[47] N. Burdet, X. Shi, D. Parks, J. N. Clark, X. Huang, et al., Opt. Express 23, 5452 (2015).
[48] J. N. Clark, X. Huang, R. Harder and I. K. Robinson, Nat. Commun. 3, 993 (2012).
[49] A. M. Maiden, M. J. Humphry and J. M. Rodenburg, J. Opt. Soc. Am. A 29, 1606 (2012).
[50] E. H. R. Tsai, I. Usov, A. Diaz, A. Menzel and M. Guizar-Sicairos, Opt. Express 24, 29089 (2016).
[51] K. Shimomura, A. Suzuki, M. Hirose and Y. Takahashi, Appl. Phys. Lett. 108, 071103 (2015).
[52] R. Horstmeyer, J. Chung, X. Ou, G. Zheng and C. Yang, Optica 3, 827 (2016).
[53] L. Tian and L. Waller, Optica 2, 104 (2015).
[54] T. B. Edo, D. J. Batey, A. M. Maiden, C. Rau, U. Wagner, et al., Phys. Rev. A 87, 53850 (2013).
[55] P. Sidorenko and O. Cohen, Optica 3, 9–14 (2016).
[56] A.-L. Robisch, K. Kröger, A. Rack and T. Salditt, New J. Phys. 17, 073033 (2015).
[57] I. Peterson, R. Harder and I. K. Robinson, Ultramicroscopy 171, 77–81 (2016).
[58] P. Ferrand, M. Allain and V. Chamard, Opt. Lett. 40, 5144 (2015).
[59] M. Odstrcil, P. Baksh, S. A. Boden, R. Card, J. E. Chad, et al., Opt. Express 24, 8360 (2016).
[60] M. Odstrcil, P. Baksh, C. Gawith, R. Vrcelj, J. G. Frey, et al., Opt. Express 24, 20245–20252 (2016).
[61] M. A. Pfeifer, G. J. Williams, I. A. Vartanyants, R. Harder and I. K. Robinson, Nature 442, 63 (2006).
[62] P. Godard, G. Carbone, M. Allain, F. Mastropietro, G. Chen, et al., Nat. Commun. 2, 568 (2011).
[63] V. Chamard, M. Allain, P. Godard, A. Talneau, G. Patriarche, et al., Scientific Reports 5, Article number: 9827 (2015).
[64] S. O. Hruszkewycz, M. Allain, M. V. Holt, C. E. Murray, J. R. Holt, et al., Nat. Mater. 16, 244–251 (2017).